Wang, S.; Zhang, H.; Yuan, J.; Yang, N.; Pang, Z.; Huang, Q. (2023) SHARK SMELL OPTIMIZATION AND DEEP LEARNING FOR INTRACRANIAL ANEURYSM DETECTION: A MODEL TAILORED FOR DIVERS AND SWIMMERS. Revista Internacional de Medicina y Ciencias de la Actividad Física y el Deporte vol. 23 (92) pp. 396-410. **DOI:** https://doi.org/10.15366/rimcafd2023.92.030

ORIGINAL

SHARK SMELL OPTIMIZATION AND DEEP LEARNING FOR INTRACRANIAL ANEURYSM DETECTION: A MODEL TAILORED FOR DIVERS AND SWIMMERS

Sen Wang[1], Hongbing Zhang[1], Jing Yuan[1], Nan Yang[1], Zhicheng Pang[1], Qing Huang[1]*

[1]Capital Medical University, Beijing LuHe hospital, Department of Neurosurgery ,101100, China

Recibido 30 de agosto de 2022 **Received** August 30, 2022
Aceptado 25 de julio de 2023 **Accepted** July 25, 2023

ABSTRACT

The detection of cerebral aneurysms, particularly among professional divers and swimmers, is crucial due to the high physical demands and pressure changes experienced in these activities. Currently, identifying these "intracranial bombs" is challenging, often leading to subarachnoid hemorrhage with high mortality and disability rates. Clipping surgery and endovascular embolization are the primary treatments, but early detection is vital for effective intervention. This study introduces the Shark Smell Optimization and Deep Learning-Enabled Automated Intracranial Aneurysms (SSODLE-AIA) model, specifically tailored for the aquatic sports community. The SSODLE-AIA model innovatively partitions cerebral aneurysms into uniform blocks, employing an EfficientNet-based feature extractor for generating feature vectors. It uniquely integrates Shark Smell Optimization (SSO) for optimal hyperparameter tuning, enhancing the model's relevance to the diving and swimming domains where sensory acuity is paramount. Furthermore, a Bidirectional Gated Recurrent Unit (BiGRU) model classifies these blocks into two types: smooth and structured. This classification is crucial for divers and swimmers, whose cerebral structures may adapt to their aquatic environments. The identification process includes mean and patch matching for these regions, ensuring high precision in detecting subtle aneurysm-related changes. The SSODLE-AIA model's effectiveness is evaluated using a cerebral aneurysm dataset. Our experimental results show that this model outperforms existing techniques, offering a promising tool for early aneurysm detection in athletes exposed to unique aquatic pressures and environments. This advancement not only aids in timely medical intervention but also contributes to the safety and longevity of careers in professional diving and swimming.

KEYWORDS: Deep Learning, Shark Smell Optimization, Intracranial Aneurysms, Gated Recurrent Unit, Feature Extraction; Diving and Swimming

1. INTRODUCTION

Exploring the depths of the ocean has always been a fascination for adventurers, marine biologists, and researchers alike. Among the many mysteries that lie beneath the waves, the detection of intracranial aneurysms—weaknesses in blood vessel walls—presents a unique challenge. The importance of timely detection of intracranial aneurysms cannot be overstated, as their rupture can lead to life-threatening hemorrhages. This is especially pertinent for divers and swimmers, who often face increased risks due to the physiological changes associated with underwater exploration. Recent advancements in deep learning and artificial intelligence have opened new horizons for medical imaging and diagnostics. Leveraging these technologies alongside nature-inspired algorithms, such as shark smell optimization, offers an innovative approach to address the specific needs of divers and swimmers. This novel model combines the sensory acuity of sharks with the analytical power of deep learning to tailor an intracranial aneurysm detection system optimized for aquatic environments. (NARANJI & KANDUL, 2017).

This study embarks on an exploration of shark smell optimization and deep learning as a collaborative approach to intracranial aneurysm detection, uniquely customized for divers and swimmers. By integrating the exceptional olfactory capabilities of sharks, which allow them to detect blood and chemical changes in water from great distances(Joo et al., 2020; Kakeda et al., 2008), with cutting-edge deep learning algorithms, we aim to create a sophisticated system capable of early aneurysm detection, even in underwater conditions. (Ivantsits, Kuhnigk, Huellebrand, Kuehne, & Hennemuth, 2021).

The implications of this research extend beyond the realm of underwater exploration and sports. It has the potential to revolutionize medical diagnostics by introducing nature-inspired sensing mechanisms and advanced AI into the medical field (Korogi et al., 1996; McDonald et al., 2015). Additionally, the development of a specialized model for divers and swimmers can significantly enhance their safety and well-being, ensuring that they can continue to explore the ocean's depths with minimized health risks. (Agid et al., 2010; Connolly Jr et al., 2012; Hemphill III et al., 2015).

In the synergy of shark smell optimization and deep learning for intracranial aneurysm detection represents a groundbreaking fusion of nature's wisdom and human ingenuity(Mensah et al., 2022). (Callagher, 2021). This model tailored for divers and swimmers promises to be a transformative development in both the fields of medical diagnostics and aquatic exploration, providing an innovative solution to a critical health challenge in a unique and exciting way.

2. RELATED WORKS

Intracranial aneurysms pose a significant health risk due to their potential for rupture, leading to life-threatening hemorrhages. Timely detection of these aneurysms is crucial for effective medical intervention and improved patient outcomes. While advancements in medical imaging have enhanced our ability to diagnose intracranial aneurysms, certain environments, such as underwater settings for divers and swimmers, present unique challenges for early detection. This literature review explores the innovative fusion of shark-inspired smell optimization and deep learning techniques to create a specialized model tailored to address the distinct needs of divers and swimmers in intracranial aneurysm detection. Sharks, as apex predators of the ocean, possess remarkable olfactory capabilities that enable them to detect blood and chemical changes in water from considerable distances. This exceptional sensory acuity has intrigued researchers for years and inspired investigations into its potential applications beyond marine biology. Recent studies have explored the idea of harnessing shark smell optimization principles for medical diagnostics, including intracranial aneurysm detection. (Ois et al., 2019; Park et al., 2019; Vlak, Algra, Brandenburg, & Rinkel, 2011).

Research in this area has shown that the keen sense of smell observed in sharks can be translated into innovative sensor technologies capable of detecting subtle chemical changes associated with aneurysm development. These studies suggest that by mimicking the principles of shark olfaction, it may be possible to create highly sensitive detectors for early signs of aneurysms. Deep learning, a subset of artificial intelligence, has gained significant traction in the field of medical imaging and diagnosis. Deep learning algorithms, particularly convolutional neural networks (CNNs), have demonstrated remarkable proficiency in recognizing patterns and anomalies in medical images. The ability to analyze complex data and identify subtle abnormalities has made deep learning an invaluable tool in various healthcare applications. (Rincon, Rossenwasser, & Dumont, 2013; Shi et al., 2020).

In the context of intracranial aneurysm detection, deep learning algorithms have shown promise in improving the accuracy and efficiency of diagnosis. These algorithms can process and interpret medical images, such as computed tomography angiography (CTA) scans and magnetic resonance angiography (MRA) images, with a high degree of precision. As a result, they have the potential to enhance the early detection of intracranial aneurysms, a critical factor in reducing associated risks. (Sichtermann et al., 2019; Sohn et al., 2021; Van Gijn, Kerr, & Rinkel, 2007).

Divers and swimmers face unique challenges when it comes to intracranial aneurysm detection. The physiological changes experienced during underwater activities, such as changes in blood pressure and oxygen levels, can complicate the interpretation of medical images. Additionally, the need for specialized equipment and expertise in underwater medicine further underscores the importance of tailored diagnostic solutions for this population. Traditional diagnostic methods may be less effective in underwater environments due to these challenges(Miki et al., 2016). Therefore, there is a pressing need to develop innovative approaches that can adapt to the specific conditions faced by divers and swimmers.

3. MATERIALS AND METHODS

In this study, a novel SSODLE-AIA model was established for effective intracranial aneurysms process. Primarily, the presented SSODLE-AIA model splits the intracranial aneurysms images into a collection of regular sized blocks. Then, the EfficientNet model is exploited to produce feature vectors and the SSO algorithm is utilized to tune the hyperparameters. Next, the BiGRU model has been used to identify the blocks into two kinds such as smooth and structured. Fig. 1 demonstrates the block diagram of SSODLE-AIA approach.

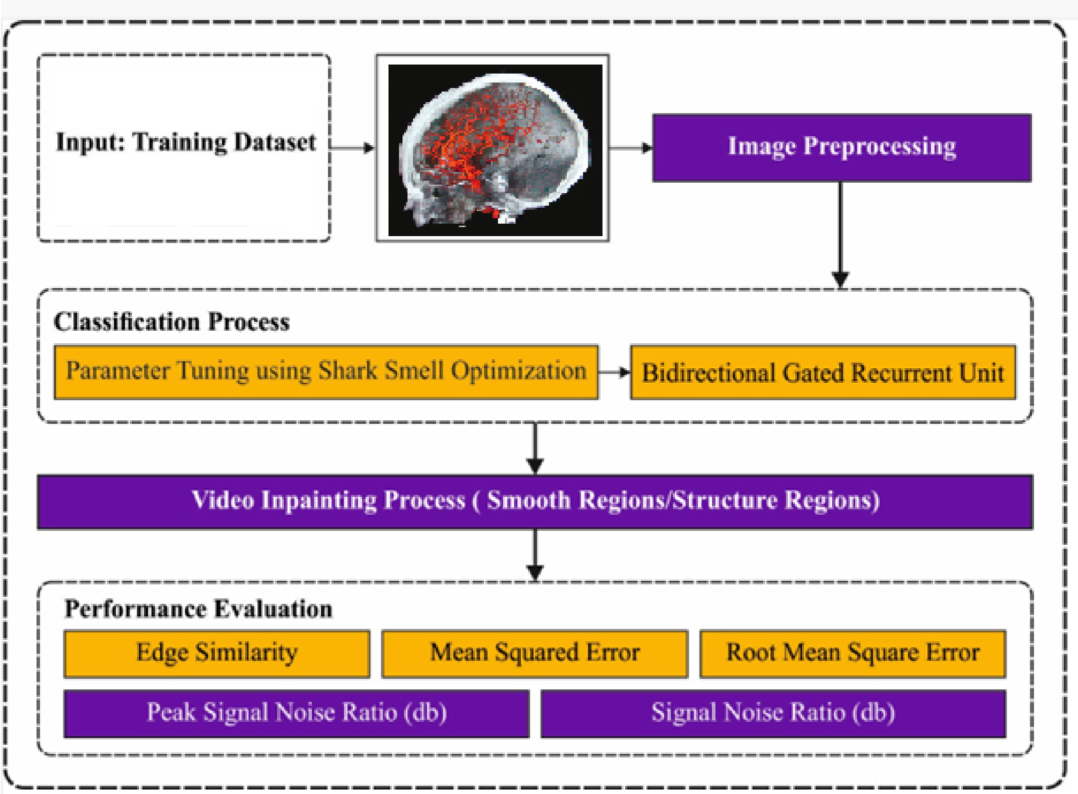

Figure 1. Block diagram of SSODLE-AIA approach

3.1. Feature Extraction

At this stage, the features involved in the uniform blocks are derived by the use of EfficientNet model. Recently, the quick development of DL approach is spawned several excellent CNN methods. From the primary easy network to existing difficult network, the efficiency of method was getting superior and superior from all the aspects (Stember et al., 2019). An EfficientNet integrates the benefit of preceding network that summarizes the progress of network efficiencies as to 3D: (i) Develop the network, i.e., utilize the skip connection for increasing the depth of NNs, and gain the feature extracting utilizing deeper layer; (ii) Extend the network, i.e., improve the count of convolutional layers for attaining further function and feature; (iii) with improving the input image resolutions, the network is expressed and learns further things that are helpful for improving accuracy. Afterward, utilize a compound co-efficient ϕ for uniformly balancing and scaling the depth, width, and resolution of network, as well as maximizing the network efficiency on restricted resources. Evaluation of compound co-efficient is provided in Eq. (1):

$$depth: d = \alpha^{\phi}$$
$$width: w = \beta^{\phi}$$
$$resolution: r = \gamma^{\phi}$$
$$s.t. \alpha \cdot \beta^2 \cdot \gamma^2 \approx 2 \ (1)$$

$$\alpha \geq 1, \beta \geq 1, \gamma \geq 1$$

In which d, w, and r signify the co-efficient utilized for scaling the depth, width, and resolution of networks. The α, β, and γ refer the resource distribution for network depth, width, and resolution. An EfficientNet mostly comprises of Stem, Dense layer, 16 Blocks, Conv2D, and GlobalAveragePooling2D. The proposal of Block was dependent on mostly the attention process and remaining infrastructure, also other infrastructures were same as standard CNN method.

3.2. Hyperparameter Optimization

As an optimum hunter in nature, the sharks have foraging nature that goes frontward and rotates viz., highly efficient in prey detection. The optimization technique simulates shark foraging is a robust optimization technique (Taufique et al., 2016; Ueda et al., 2019). For a particular location, the shark moves at a fast speed toward the particles that have strong odor concentration, thus the velocity vector is formulated by the following equation.

$$[V_1^1, V_2^1, \dots, V_{NP}^1] \ (2)$$

The sharks possess inertia when it swims, therefore the velocity equation of every single dimension is formulated by the given expression,

$$V_{i,j}^k = \eta_k \cdot R_1 \cdot \left.\frac{\partial(OF)}{\partial x_j}\right|_{x_{i,j}^k} + \alpha_k \cdot R_2 \cdot v_{i,j}^{k-1} \ (3)$$

In Eq. (3), $j = (1,2,\cdots,ND), i = (1,2,\cdots,NP)$, and $k = (1,2,\cdots,k_{\max})$; ND refers to the dimension amount; NP characterizes the velocity vector count (size of shark populations); $k_{\max}$ embodies the iteration amount; *OF* signifies the objective function; $\eta_k \in [0,1]$ epitomize the gradient co-efficient; a_k characterize the weight co-efficient, besides, it is an arbitrary integer lie within [0,1], also R_1 & R_2 represented as two arbitrary values ranging from [0,1].
The speed of shark is essential for preventing the boundary and speed limit in the following,

$$\left|v_{i,j}^k\right| = \min\left[\left|v_{i,j}^k\right|, \left|\beta_k \cdot v_{i,j}^{k-1}\right|\right] \ (4)$$

In Eq. (4), β_k characterize the speed limiting factor of k-th iterations. The shark possesses a novel location Y_i^{k+1} because of forwarding movement, and Y_i^{k+1} is defined by the preceding location and speed that is represented by

$$Y_i^{k+1} = X_i^k + V_i^k \cdot \Delta t_k \ (5)$$

In Eq. (5), Δt_k refers to the time interval of k-th iteration. Also moving forward, sharks generally rotate along with the path to seek stronger odor particles and improve the motion direction, that is, actual direction of moving. The rotating shark moves in a closed range that is basically not a circle. In the optimization view, shark performs local searching at each stage to detect best solution candidate. The searching equation is given by,

$$Z_i^{k+1,m} = Y_i^{k+1} + R3 \cdot Y_i^{k+1} \ (6)$$

In Eq. (6), $m = (1, 2, \cdots, M)$ indicates the number of points at every stage of searching location; R_3 characterize the arbitrary value within $[-1, 1]$. Once the sharks find a strong odor point in the rotation, they move to the point and continue the search direction. The search procedure for this location is represented as follows,

$$X_i^{k+1} = \arg\max\{OF(Y_i^{k+1}), OF(Z_i^{k+1,1}), \ldots, OF(Z_i^{k+1,M})\} \ (7)$$

As aforementioned, Y_i^{k+1} is acquired from the linear motion and $Z_i^{k+1,M}$ is achieved from the rotational motion. Fig. 2 depicts the flowchart of SSO algorithm.

Figure 2. Flowchart of SSO algorithm

ALGORITHM 1: PSEUDOCODE OF SSO ALGORITHM
Pseudo-Code of SSO
Begin
Step 1. Initialize parameters
Assume parameters $NP, k_{\max}, \eta k, \alpha k$, and $\beta_k (k = 1,2, k_{\max})$
Produce primary population with every individual
Arbitrarily produce all decisions in the permissible range
Stage counter initialization $k = 1$
For = 1 : $k_{\max}$
Step 2. Forward motion
Determine every element of velocity vector,
$v_{i,j}(i = 1, \ldots, NP, j = 1, \ldots, ND)$
Attain new shark location using forward motion, $Y_i^{k+1}(i = 1, \ldots, NP)$
Step 3. Rotation motion
Attain new shark location using rotational motion, $z_i^{k+1,m}(m = 1, .., M)$
Choose succeeding location of shark using two motions $X_i^{k+1}(i = 1, \ldots, NP)$
End for k
Set $k = k + 1$
Pick optimal shark location in the final state that includes maximum OF value.
End

The SSO approach grows a fitness function (FF) for achieving enhanced classifier efficiency. It defines a positive integer for representing the superior efficiency of candidate outcomes. During this case, minimize classifier error rate has been regarded as FF is obtainable in Eq. (8).

$$fitness(x_i) = ClassifierErrorRate(x_i) = \frac{number\ of\ misclassified\ blocks}{Total\ number\ of\ blocks} * 100 \quad (8)$$

3.3. BiGRU based Smooth and Structured Block Classification

GRU is extremely same as LSTM, however, it implements gate process for tracking the state of order before utilizing a distinct storing unit that creates the infrastructure easier [20]. It comprises 2 types of gates such as reset gate r_r and update gate z_r. It is control that data was upgraded to state together. r_r control the influence of past state to candidate state $\tilde{h}$, and lesser their value is further it can be ignored. At time f, r_t was upgraded as:

$$r_t = \sigma(U_r x_t + W_r h_{t-1} + b_r) \quad (9)$$

whereas σ refers the sigmoid function, x_l and h_{t-1} correspondingly implies the input and preceding hidden state. z_t has been utilized for controlling several past data was recollected and several novel data is occupied. The superior the value is, the further status data at the preceding moment was taken in. z_t was upgraded as:

$$z_t = \sigma(U_Z x_t + 1W_Z h_{t-1} + b_z) \quad (10)$$

The state of GRU at time t was calculated as the subsequent formula:

$$h_r = (1 - z_r) \odot \tilde{h} + z_r \odot h_{t-1} \quad (11)$$

whereas $\odot$ implies the vector element multiplication and candidate state $\tilde{h}$ has calculated as:

$$\tilde{h} = \tanh\left(U_h x_f + \frac{1}{V_h\left(h_{f-1} \odot r_t\right)} + b_h\right) \quad (12)$$

and U_r, W_r, U_Z, W_Z, U_h and W_h in (9) (10) (12) are learnable weighted, b_h, b_r, and b_Z are bias terms. But the conventional RNNs only utilize the previous data, the bidirectional RNN (BRNN) is procedure information in both directions. The outcome y of BRNN is attained by calculating the forward hidden order $\overrightarrow{h_r}$ and backward order $\overleftarrow{h_t}$ from iterative approach utilizing the subsequent formulas:

$$\vec{h}_t = \Phi\left(WW_{\chi\vec{h}} x_t + W_{\vec{h}\vec{h}} \vec{h}_{t-1} + b_{\vec{h}}\right) \quad (13)$$

$$\overleftarrow{h_t} = \Phi\left(W_{x\overleftarrow{h}} x_t xh + W_{\overleftarrow{h}\overleftarrow{h}} \overleftarrow{h}_{t-1} + b_{\overleftarrow{h}}\right) \quad (14)$$

$$y_t = W_{\vec{h}y} \vec{h}_t + W_{\overleftarrow{h}y} \overleftarrow{h}_{t-1} + b_y \quad (15)$$

Relating BRNN with GRU provides BGRU that is utilized for accessing the long-term full sequential data of provided order from both directions. While a fault analysis problem is usually noticed as a classifier problem, cross-entropy was implemented as the loss function. While the instance was weighted, the weighted cross-entropy was offered as:

$$f(\theta) = -\sum_{n=1}^{N} w_n \sum_{i=1}^{M} y_i \, 1og(\hat{y}_i) \ (16)$$

whereas θ signifies the NN parameters, N signifies the amount of instances, M stands for the count of faults, y_i indicates the true label and $\hat{y}_i$ implies the predictive probability. At the time of training the BiGRU method, it maintains the target as smoothing or infrastructure depending on the standard deviation (SD) of certain blocks. If the SD develops lesser than 5, the target was preserved as smooth one. Else, it can be assumed that infrastructure area is offered under.

$$type = \begin{cases} structure \ if \ SD > 5 \\ smooth \ otherwise \end{cases} \ (17)$$

4. PERFORMANCE VALIDATION

In this section studies the performance of the SSODLE-AIA algorithm employing MATLAB tool against identified dataset [22]. A few sample sequences are illustrated in Fig. 3.

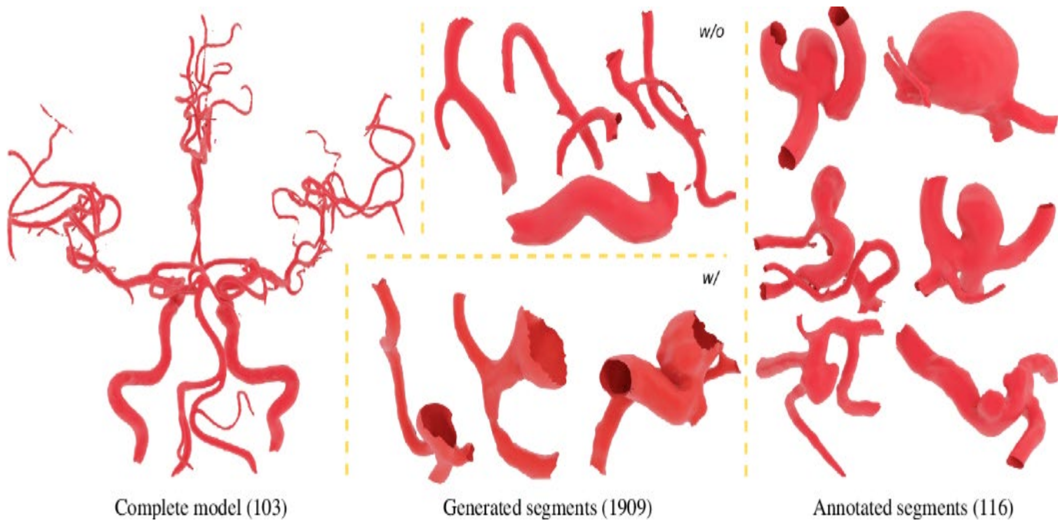

Figure 3. Sample intracranial aneurysms images

Table 1 and Fig. 4 provide a comparative edge similarity (ESIM) outcome of the SSODLE-AIA model with existing models. The experimental results indicated that the SSODLE-AIA model has gained effectual performance with maximum values of ESIM.

For instance, in image 1, the SSODLE-AIA model has offered increased ESIM of 112 whereas the GWO, CSA, MVO, CS-MVO, and VIA-BASDBN models have accomplished reduced ESIM of 101, 102, 103, 106, and 108 respectively. In addition, in image 3, the SSODLE-AIA approach has accessible improved ESIM of 70 whereas the GWO, CSA, MVO, CS-MVO, and VIA-BASDBN systems have accomplished lower ESIM of 52, 56, 58, 61, and 65 correspondingly.

Moreover, in image 4, the SSODLE-AIA algorithm has offered maximal ESIM of 118 whereas the GWO, CSA, MVO, CS-MVO, and VIA-BASDBN models have accomplished minimal ESIM of 100, 101, 102, 105, and 110 correspondingly.

Table 1 ESIM analysis of SSODLE-AIA algorithm with existing approaches under four test images

EDGE SIMILARITY						
DATASET	**GWO MODEL**	**CSA MODEL**	**MVO MODEL**	**CS-MVO MODEL**	**VIA-BASDBN**	**SSODLE-AIA**
Image 1	101	102	103	106	108	112
Image 2	125	130	133	135	138	140
Image 3	52	56	58	61	65	70
Image 4	100	101	102	105	110	118

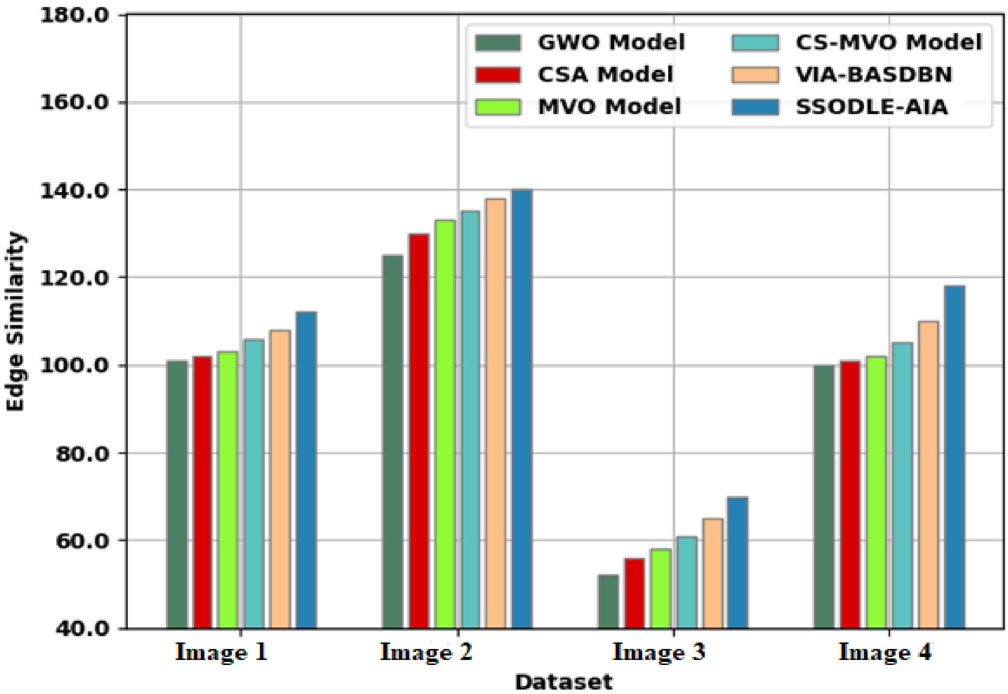

Figure 4. ESIM analysis of SSODLE-AIA technique under four test images

A comparative MSE inspection of the SSODLE-AIA model with existing models under four test images is shown in Table 2 and Fig. 5. The simulation outcomes reported that the SSODLE-AIA model has revealed effectual outcomes with least values of MSE. For instance, in image 1, the SSODLE-AIA model has gained least MSE of 32.51 whereas the GWO, CSA, MVO, CS-MVO, and VIA-BASDBN models have resulted in increased MSE of 64.43, 64.24, 59.04, 58.85, and 57.35 respectively.

Also, in image 3, the SSODLE-AIA system has attained minimal MSE of

18.67 whereas the GWO, CSA, MVO, CS-MVO, and VIA-BASDBN approaches have resulted in enhanced MSE of 38.45, 37.10, 29.02, 26.71, and 22.84 respectively. Then, in image 4, the SSODLE-AIA approach has reached lower MSE of 8.14 whereas the GWO, CSA, MVO, CS-MVO, and VIA-BASDBN approaches have resulted in superior MSE of 12.86, 12.66, 13.63, 12.28, and 10.22 correspondingly.

Table 2 MSE analysis of SSODLE-AIA algorithm with existing approaches under four test images

MEAN SQUARED ERROR						
DATASET	**GWO MODEL**	**CSA MODEL**	**MVO MODEL**	**CS-MVO MODEL**	**VIA-BASDBN**	**SSODLE-AIA**
Image 1	64.43	64.24	59.04	58.85	57.35	32.51
Image 2	54.81	56.92	53.46	52.11	49.12	45.31
Image 3	38.45	37.10	29.02	26.71	22.84	18.67
Image 4	12.86	12.66	13.63	12.28	10.22	8.14

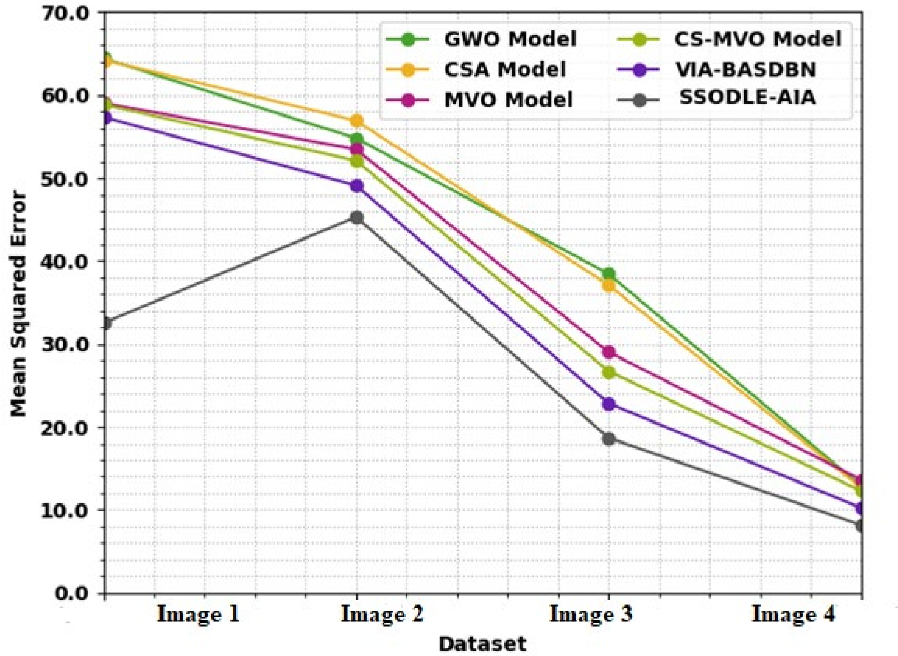

Figure 5. MSE analysis of SSODLE-AIA algorithm

A comparative RMSE examination of the SSODLE-AIA approach with existing algorithms under four test images is exposed in Table 3 and Fig. 6. The simulation outcomes reported that the SSODLE-AIA model has shown effectual outcomes with least values of RMSE. For instance, in image 1, the SSODLE-AIA system has gained least RMSE of 5.70 whereas the GWO, CSA, MVO, CS-MVO, and VIA-BASDBN models have resulted in increased RMSE of 8.03, 8.01, 7.68, 7.67, and 7.57 correspondingly.

Likewise, in image 3, the SSODLE-AIA algorithm has gained least RMSE of 4.32 whereas the GWO, CSA, MVO, CS-MVO, and VIA-BASDBN systems have resulted in enhanced RMSE of 6.20, 6.09, 5.39, 5.17, and 4.78 correspondingly. Eventually, in image 4, the SSODLE-AIA system has gained least RMSE of 2.85 whereas the GWO, CSA, MVO, CS-MVO, and VIA-BASDBN methodologies have resulted in maximal RMSE of 3.59, 3.56, 3.69, 3.50, and 3.20 correspondingly.

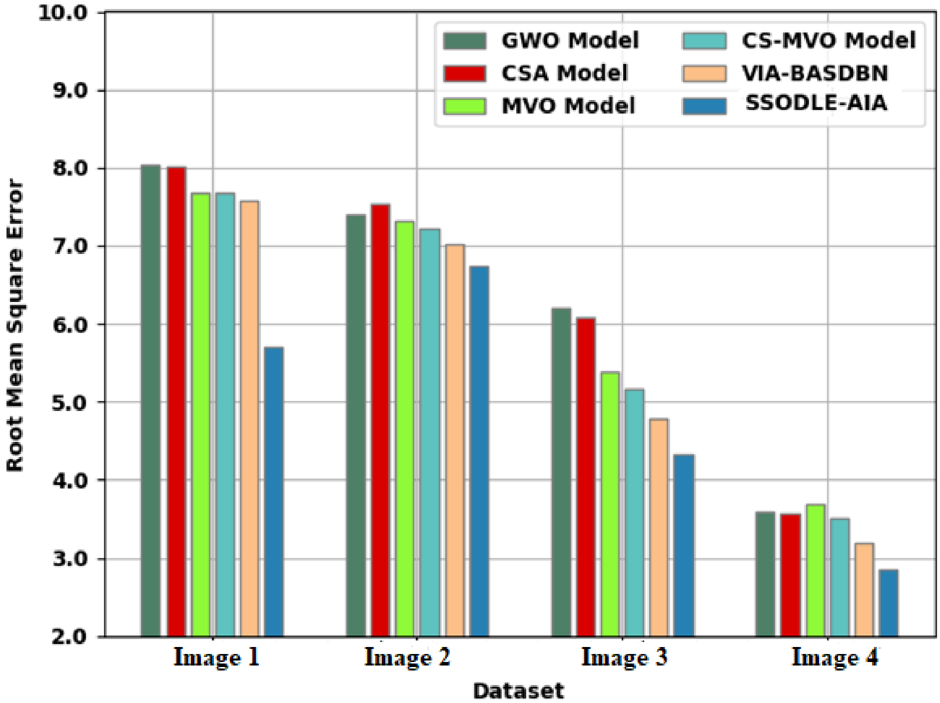

Figure 6. RMSE analysis of SSODLE-AIA technique under four test images

Table 3 RMSE analysis of SSODLE-AIA algorithm with existing approaches

ROOT MEAN SQUARE ERROR						
DATASET	**GWO MODEL**	**CSA MODEL**	**MVO MODEL**	**CS-MVO MODEL**	**VIA-BASDBN**	**SSODLE-AIA**
Image 1	8.03	8.01	7.68	7.67	7.57	5.70
Image 2	7.40	7.54	7.31	7.22	7.01	6.73
Image 3	6.20	6.09	5.39	5.17	4.78	4.32
Image 4	3.59	3.56	3.69	3.50	3.20	2.85

Table 4 and Fig. 7 illustrate a comparative PSNR outcome of the SSODLE-AIA approach with existing models. The experimental results indicated that the SSODLE-AIA system has gained effectual performance with maximal values of PSNR.

For instance, on image 1, the SSODLE-AIA system has obtainable higher PSNR of 33.01dB whereas the GWO, CSA, MVO, CS-MVO, and VIA-BASDBN algorithms have accomplished reduced PSNR of 30.04dB, 30.05dB, 30.42dB, 30.43dB, and 30.55dB correspondingly. Additionally, in image 3, the SSODLE-AIA model has offered maximal PSNR of 35.42dB whereas the GWO, CSA, MVO, CS-MVO, and VIA-BASDBN techniques have accomplished reduced PSNR of 32.28dB, 32.44dB, 33.50dB, 33.86dB, and 34.54dB correspondingly. At last, on image 4, the SSODLE-AIA methodology has accessible improved PSNR of 39.02dB whereas the GWO, CSA, MVO, CS-MVO, and VIA-BASDBN algorithms have accomplished reduced PSNR of 37.04dB, 37.11dB, 36.79dB, 37.24dB, and 38.04dB correspondingly.

Table 4 PSNR analysis of SSODLE-AIA technique with existing approaches

PEAK SIGNAL NOISE RATIO (DB)						
DATASET	**GWO MODEL**	**CSA MODEL**	**MVO MODEL**	**CS-MVO MODEL**	**VIA-BASDBN**	**SSODLE-AIA**
Image 1	30.04	30.05	30.42	30.43	30.55	33.01
Image 2	30.74	30.58	30.85	30.96	31.22	31.57
Image 3	32.28	32.44	33.50	33.86	34.54	35.42
Image 4	37.04	37.11	36.79	37.24	38.04	39.02

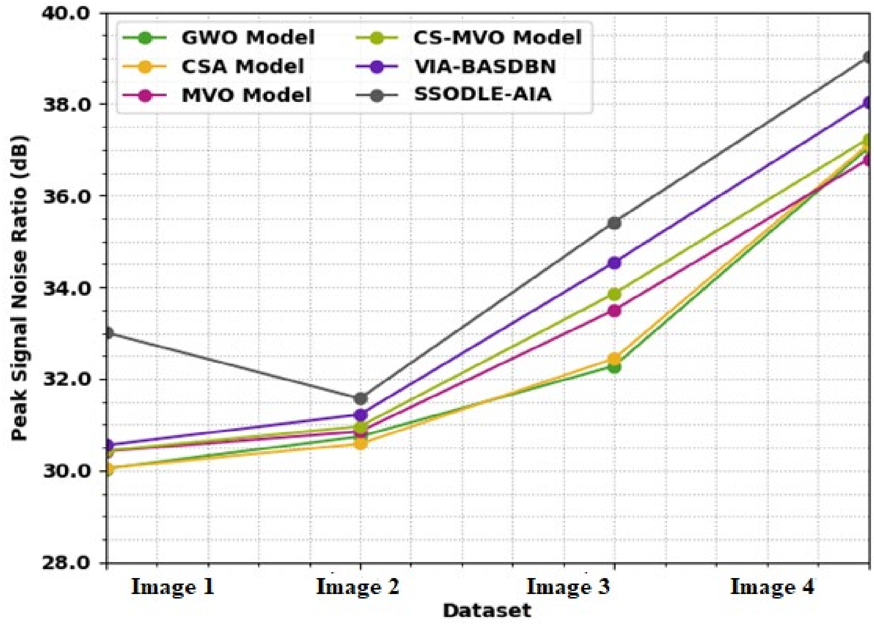

Figure 7. PSNR analysis of SSODLE-AIA technique

Table 5 and Fig. 8 demonstrate a comparative SNR outcome of the SSODLE-AIA system with existing models. The experimental results indicated that the SSODLE-AIA approach has gained effectual performance with maximal values of SNR. For instance, in image 1, the SSODLE-AIA model has offered increased SNR of 18dB whereas the GWO, CSA, MVO, CS-MVO, and VIA-BASDBN models have accomplished reduced SNR of 13dB, 13dB, 15dB, 15dB, and 15dB respectively. Similarly, in image 3, the SSODLE-AIA algorithm has offered increased SNR of 17dB whereas the GWO, CSA, MVO, CS-MVO, and VIA-BASDBN methodologies have accomplished lesser SNR of 14dB, 14dB, 15dB, 16dB, and 16dB correspondingly. Lastly, in image 4, the SSODLE-AIA approach has obtainable increased SNR of 17dB whereas the GWO, CSA, MVO, CS-MVO, and VIA-BASDBN models have accomplished reduced SNR of 14dB, 14dB, 14dB, 14dB, and 15dB correspondingly.

Table 5 SNR analysis of SSODLE-AIA technique with existing approaches

SIGNAL NOISE RATIO (DB)						
DATASET	**GWO MODEL**	**CSA MODEL**	**MVO MODEL**	**CS-MVO MODEL**	**VIA-BASDBN**	**SSODLE-AIA**
Image 1	13.00	13.00	15.00	15.00	15.00	18.00
Image 2	13.00	13.00	13.00	13.00	14.00	17.00
Image 3	14.00	14.00	15.00	16.00	16.00	17.00
Image 4	14.00	14.00	14.00	14.00	15.00	17.00

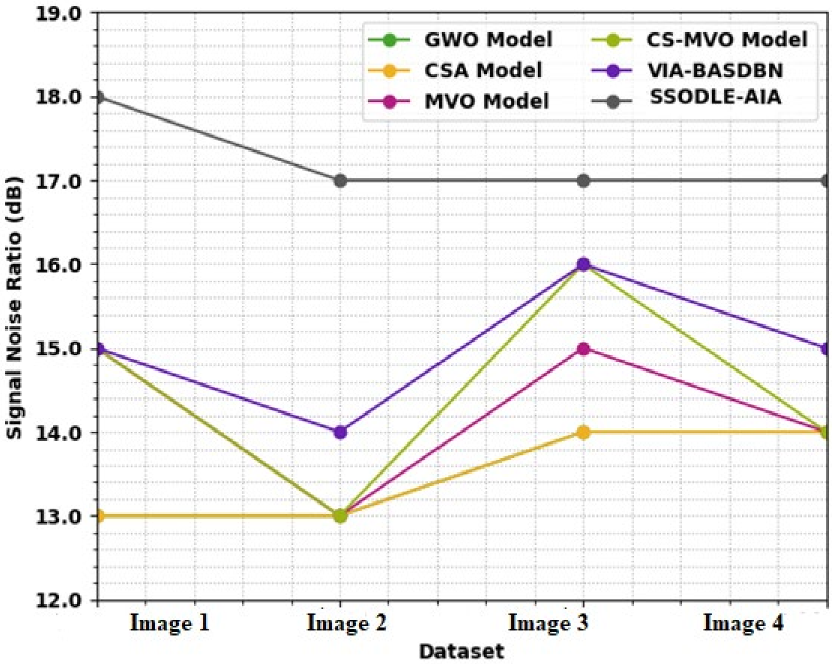

Figure 8. SNR analysis of SSODLE-AIA technique

From these results and discussion, it is obvious that the SSODLE-AIA model has showcased maximal intracranial aneurysms detection performance over other models.

5. CONCLUSION

In conclusion, the fusion of shark smell optimization and deep learning for intracranial aneurysm detection represents a pioneering approach tailored for divers and swimmers. This innovative model holds the potential to significantly enhance early detection capabilities in challenging underwater environments, addressing a critical health concern in these unique settings. The convergence of nature-inspired sensory acuity and advanced artificial intelligence showcases the potential for transformative advancements in medical diagnostics, opening up new avenues for interdisciplinary collaboration and exploration beneath the waves.

REFERENCES

Agid, R., Andersson, T., Almqvist, H., Willinsky, R., Lee, S.-K., Farb, R., & Söderman, M. (2010). Negative CT angiography findings in patients with spontaneous subarachnoid hemorrhage: when is digital subtraction angiography still needed? *American Journal of Neuroradiology, 31*(4), 696-705.

Callagher, L. (2021). Bioentrepreneurship education: where have we been and where to next? *Journal of Commercial Biotechnology, 26*(3).

Connolly Jr, E. S., Rabinstein, A. A., Carhuapoma, J. R., Derdeyn, C. P., Dion, J., Higashida, R. T., . . . Ogilvy, C. S. (2012). Guidelines for the management of aneurysmal subarachnoid hemorrhage: a guideline for healthcare professionals from the American Heart Association/American Stroke Association. *Stroke, 43*(6), 1711-1737.

Hemphill III, J. C., Greenberg, S. M., Anderson, C. S., Becker, K., Bendok, B. R., Cushman, M., . . . Mitchell, P. H. (2015). Guidelines for the management of spontaneous intracerebral hemorrhage: a guideline for healthcare professionals from the American Heart Association/American Stroke Association. *Stroke, 46*(7), 2032-2060.

Ivantsits, M., Kuhnigk, J.-M., Huellebrand, M., Kuehne, T., & Hennemuth, A. (2021). *Deep Learning-Based 3D U-Net Cerebral Aneurysm Detection.* Paper presented at the Cerebral Aneurysm Detection and Analysis: First Challenge, CADA 2020, Held in Conjunction with MICCAI 2020, Lima, Peru, October 8, 2020, Proceedings 1.

Joo, B., Ahn, S. S., Yoon, P. H., Bae, S., Sohn, B., Lee, Y. E., . . . Lee, S.-K. (2020). A deep learning algorithm may automate intracranial aneurysm detection on MR angiography with high diagnostic performance. *European Radiology, 30*, 5785-5793.

Kakeda, S., Korogi, Y., Arimura, H., Hirai, T., Katsuragawa, S., Aoki, T., & Doi, K. (2008). Diagnostic accuracy and reading time to detect intracranial aneurysms on MR angiography using a computer-aided diagnosis system. *American Journal of Roentgenology, 190*(2), 459-465.

Korogi, Y., Takahashi, M., Mabuchi, N., Nakagawa, T., Fujiwara, S., Horikawa, Y., . . . Shiokawa, Y. (1996). Intracranial aneurysms: diagnostic accuracy of MR angiography with evaluation of maximum intensity projection and source images. *Radiology, 199*(1), 199-207.

McDonald, R. J., Schwartz, K. M., Eckel, L. J., Diehn, F. E., Hunt, C. H., Bartholmai, B. J., . . . Kallmes, D. F. (2015). The effects of changes in utilization and technological advancements of cross-sectional imaging on radiologist workload. *Academic Radiology, 22*(9), 1191-1198.

Mensah, E., Pringle, C., Roberts, G., Gurusinghe, N., Golash, A., & Alalade, A. F. (2022). Deep Learning in the Management of Intracranial Aneurysms and Cerebrovascular Diseases: A Review of the Current Literature. *World Neurosurgery*.

Miki, S., Hayashi, N., Masutani, Y., Nomura, Y., Yoshikawa, T., Hanaoka, S., . . . Ohtomo, K. (2016). Computer-assisted detection of cerebral aneurysms in MR angiography in a routine image-reading environment: effects on diagnosis by radiologists. *American Journal of Neuroradiology, 37*(6), 1038-1043.

NARANJI, M. K., & KANDUL, S. (2017). Australian sawcheek scorpionfish, Brachypterois curvispina Matsunuma, Sakurai & Motomura 2013 (Scorpaeniformes: Scorpaenidae) new record from Indian waters. *FishTaxa, 2*(2), 71-75.

Ois, A., Vivas, E., Figueras-Aguirre, G., Guimaraens, L., Cuadrado-Godia, E., Avellaneda, C., . . . Villalba, G. (2019). Misdiagnosis worsens prognosis in subarachnoid hemorrhage with good Hunt and Hess score. *Stroke, 50*(11), 3072-3076.

Park, A., Chute, C., Rajpurkar, P., Lou, J., Ball, R. L., Shpanskaya, K., . . . Tseng, J. (2019). Deep learning–assisted diagnosis of cerebral aneurysms using the HeadXNet model. *JAMA network open, 2*(6), e195600-e195600.

Rincon, F., Rossenwasser, R. H., & Dumont, A. (2013). The epidemiology of admissions of nontraumatic subarachnoid hemorrhage in the United States. *Neurosurgery, 73*(2), 217-223.

Shi, Z., Miao, C., Schoepf, U. J., Savage, R. H., Dargis, D. M., Pan, C., . . . Zhang, X. (2020). A clinically applicable deep-learning model for detecting intracranial aneurysm in computed tomography angiography images. *Nature communications, 11*(1), 6090.

Sichtermann, T., Faron, A., Sijben, R., Teichert, N., Freiherr, J., & Wiesmann, M. (2019). Deep learning–based detection of intracranial aneurysms in 3D TOF-MRA. *American Journal of Neuroradiology, 40*(1), 25-32.

Sohn, B., Park, K.-Y., Choi, J., Koo, J., Han, K., Joo, B., . . . Lee, S.-K. (2021). Deep Learning–Based Software Improves Clinicians' Detection Sensitivity of Aneurysms on Brain TOF-MRA. *American Journal of Neuroradiology, 42*(10), 1769-1775.

Stember, J. N., Chang, P., Stember, D. M., Liu, M., Grinband, J., Filippi, C. G., . . . Jambawalikar, S. (2019). Convolutional neural networks for the detection and measurement of cerebral aneurysms on magnetic resonance angiography. *Journal of digital imaging, 32*, 808-815.

Taufique, Z., May, T., Meyers, E., Falo, C., Mayer, S. A., Agarwal, S., . . . Schmidt, J. M. (2016). Predictors of poor quality of life 1 year after subarachnoid hemorrhage. *Neurosurgery, 78*(2), 256-264.

Ueda, D., Yamamoto, A., Nishimori, M., Shimono, T., Doishita, S., Shimazaki, A., . . . Shimahara, Y. (2019). Deep learning for MR angiography: automated detection of cerebral aneurysms. *Radiology, 290*(1), 187-194.

Van Gijn, J., Kerr, R. S., & Rinkel, G. J. (2007). Subarachnoid haemorrhage. *The Lancet, 369*(9558), 306-318.

Vlak, M. H., Algra, A., Brandenburg, R., & Rinkel, G. J. (2011). Prevalence of unruptured intracranial aneurysms, with emphasis on sex, age, comorbidity, country, and time period: a systematic review and meta-analysis. *The Lancet Neurology, 10*(7), 626-636.